

SIMULATIONS AND VERIFICATIONS OF TRUE 3D OPTICAL PARTS BY INJECTION MOLDING PROCESS

Yuan-Jung Chang¹, Chao-Kai Yu¹, Hsien-Sen Chiu¹, Wen-Hsien Yang¹, Huai-En Lai² and Pei-Jen Wang²

1. CoreTech System (Moldex3D) Co., Ltd., ChuPei City, Hsinchu, 30265, Taiwan

2. Department of Power Mechanical Engineering, National Tsing Hua University, Hsinchu 30013, Taiwan

Abstract

Injection-molded optical parts have been widely employed for various commercial electronic products in the market today. The large variations in thickness and stringent requirements in residual stresses have made the parts tough to manufacture. In this study, a true 3D CAE analysis incorporated with visco-elasticity models have been adopted for studies of typical cases. Some interesting phenomena during filling and packing of the parts have been predicted by the CAE simulations. Furthermore, experimental verifications on the phenomena have been conducted with reasonable accuracy not only in form accuracy but in residual stresses. Finally, the results have shown that residual stresses are mainly due to melt and injection speed whereas dimensional errors on part-surfaces are dependent of holding pressure and melt temperature during the molding process.

Introduction

As progress in optical technology was made in the past few decades, optical lens systems are commonly applied to numerous consumer products in our daily life. Since consumer products must be mass-produced in millions of unit in the life expectancy, it is necessary to adopt a manufacture process that can produce the products both in good quality and at affordable prices. Among the most popular manufacture processes, injection molding process has been widely accepted in the industries because its ability to meet the above production requirements. It is therefore essential for the plastics industry to comprehend the sophisticate process for injection-molded plastics lenses.

It has been noted that, in injection molding of plastics lenses, the qualities of optical image are affected by crucial factors generally classified into two categories, namely geometric features and optical birefringence. The geometric features, namely profile accuracy and volumetric deviations, are influenced by pertinent processing parameters during injection molding. These dimensional errors eventually contribute to optical aberrations in object

images, or called Seidel aberrations, including spherical aberration, coma, astigmatism, field curvature, and distortion. On the other hand, the residual birefringence in lenses defocuses and blurs object images supposed to be clear and sharp. Based upon the photo-elasticity theory, it is noted that two mechanisms are credited to the residual birefringence in materials, namely the flow-induced and thermal-induced birefringence, during the injection molding process [1,2]. The former is attributed to molecular-chain orientation generated by shear stresses during the filling and holding stages, and can be relaxed or frozen during post-filling processes and after ejection. The latter is contributed by internal stresses due to spatial non-uniform shrinkage, which is caused by each specific location inside the part has its unique thermo-mechanical history in temperature and pressure.

According to the previous researches done by Wang et al. [3,4], residual birefringence in COC molded lenses is contributed mostly by flow-induced effects because the flow-induced birefringence accounts for 92 % as compared to the thermal-induced parts being 8 %. Hence, to further comprehend flow-induced birefringence in this paper, a true 3D CAE analysis incorporated with visco-elasticity models was adopted to investigate birefringence of COC molded lenses in details. Experimental investigations were also conducted for correlating causal effects between processing conditions and birefringence levels.

CAE Simulation

In this study, a commercial CAE analysis program, Moldex3D copyrighted by CoreTech System at Hsinchu, Taiwan, has been adopted as the analysis tool on simulating the flow phenomena of polymeric melt inside the mold cavity during the process. The polymer melt is assumed to be modeled as a visco-elastic fluid. Therefore, the non-isothermal 3D flow motion can be mathematically described in the following equations:

$$\frac{\partial \rho}{\partial t} + \nabla \cdot \rho \mathbf{u} = 0, \quad (1)$$

$$\frac{\partial}{\partial t}(\rho \mathbf{u}) + \nabla \cdot (\rho \mathbf{u} \mathbf{u} - \boldsymbol{\sigma}) = \rho \mathbf{g}, \quad (2)$$

$$\boldsymbol{\sigma} = -p \mathbf{I} + \boldsymbol{\tau}, \quad (3)$$

$$\rho C_p \left(\frac{\partial T}{\partial t} + \mathbf{u} \cdot \nabla T \right) = \nabla \cdot (\mathbf{k} \nabla T) + \frac{1}{2} \boldsymbol{\tau} : (\nabla \mathbf{u} + \nabla \mathbf{u}^T), \quad (4)$$

where u is the velocity vector, T is the temperature, t is the time, p is the pressure, $\boldsymbol{\sigma}$ is the total stress tensor, ρ is the density, $\boldsymbol{\tau}$ is the extra-stress tensor, k is the thermal conductivity, and C_p is the specific heat. In present work, $\boldsymbol{\tau}$ is obtained by the constitutive equation of White-Metzner model as follows:

$$\boldsymbol{\tau} + \lambda \overset{\nabla}{\boldsymbol{\tau}} = \eta (\nabla \mathbf{u} + \nabla \mathbf{u}^T), \quad (5)$$

where λ is the relaxation time, and η is the viscosity; λ and η are both functions of shear rate and temperature.

In optical plastics, the value of refractive index varies as a function of the applied-stresses. This is further described by the Stress-Optic, or ‘‘Brewster’s’’ Law denoted in the following equation:

$$n_1 - n_2 = C_B (\sigma_1 - \sigma_2), \quad (6)$$

where n_1 and n_2 are the indices of refraction, σ_1 and σ_2 are the principal stresses, and C_B is the Stress-optical constant. This law describes that birefringence is directly proportional to the difference of principal stresses.

The phase difference between the two light rays traveling through the material at different velocities is known as retardation, δ . The retardation value divided by the thickness of material, d , is proportional to the difference between the two indices of refraction, i.e.,

$$\delta = \Delta n d. \quad (7)$$

The fringe order, N , can be determined by ratio of the retardation value to the wavelength of light, λ , as the following equation:

$$\frac{\delta}{\lambda} = N. \quad (8)$$

In the CAE simulations, a spherical lens in plano-convex geometry with curvature in 70 mm, diameter in 32 mm, thickness in 2 mm, and gate thickness in 0.80 mm was molded for experimental verifications as shown in Fig. 1 with corresponding process conditions being listed in Table 1.

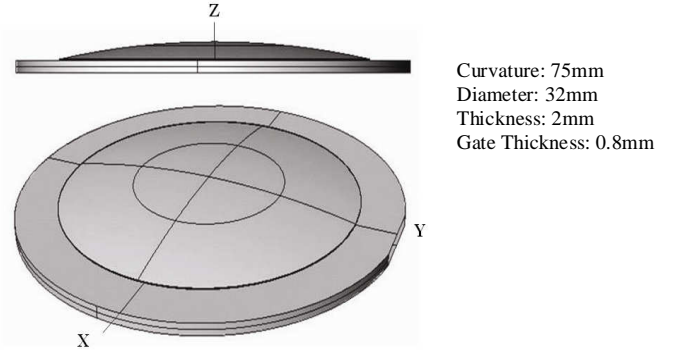


Fig. 1 Schematic drawings of the plano-convex spherical lens with gate located at the Y axis.

Table 1 Processing conditions for the case of plano-convex spherical lens mold.

	Clamping force	550	kN
	Injection weight	27	Gm
	Max. Pre.	259	Mpa
Machine	Max. Flow	190	cc/sec
Conditions	Screw diameter	22	Mm
	Stroke	70	Mm
	Injection speed	22	mm/sec
	Holding pres.	98.10	Mpa
	Cooling time	60	Sec
Mold	Open time	8.76	Sec
Conditions	Coolant	Silicone oil	
	Rom temp.	25	°C
	Resins	Zeonex 480R	
Melt	Melt temp.	275	°C
Conditions	Mold temp.	124	°C
	Ejecting temp.	127	°C

The simulated fringe patterns are shown in Fig 2. The distributions of flow-induced fringe pattern as shown in Fig. 2(a) are similar to the maximum shear stresses at the end of filling stage as shown in Fig. 3. The rationale for this result is the high flow-induced residual stresses would concentrate at the lens gate and near the mold walls. The distributions of thermal-induced fringe pattern as shown in Fig. 2(b) are in concentric circles with indistinct increments. This might be attributed to the spatial non-uniform shrinkage caused by the polymer at melt core shrinking more than the others. Furthermore, comparing Fig. 2(a) with Fig. 2(b), it is noted that flow-induced fringe order is significantly larger than thermal-induced fringe order. In terms of birefringence based upon simulated predictions, the plastics lenses molded by ZEONEX 480R are mainly exhibiting flow-induced birefringence; and, they do not show noticeable thermal-induced birefringence.

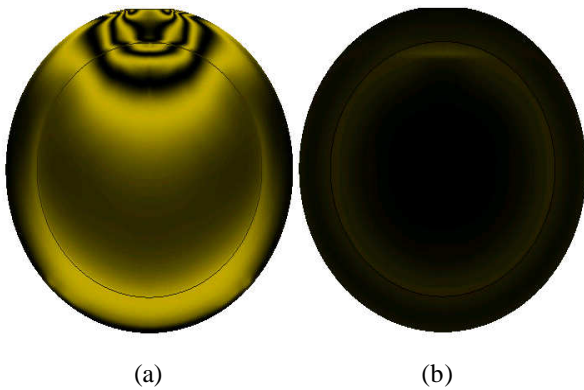


Fig. 2 Plots of fringe pattern caused by different stress effects for the case of plano-convex lens; (a) birefringence due to flow-induced stresses; (b) birefringence due to thermal-induced stresses.

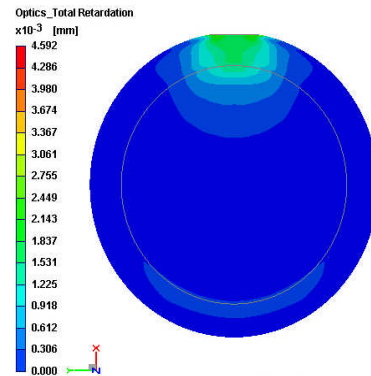


Fig. 4 Color-shaded plots of predicted optical retardation distributions after cooling stage for the case of plano-convex lens.

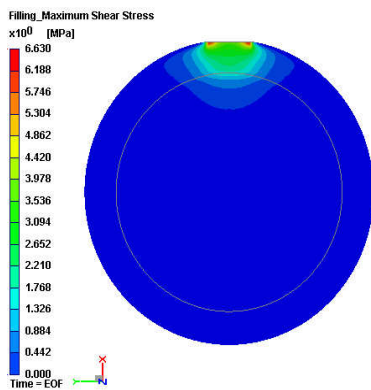


Fig. 3 Color-shaded plots of maximum shear-stress distribution for the case of plano-convex lens at the end of filling stage.

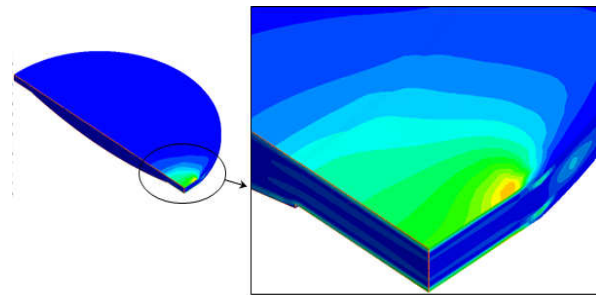


Fig. 5 Color-shaded plots of birefringence in gap-wise direction with maximum peak values of birefringence occurring near the mold wall; and the second peak-values of birefringence near the central part of gap for the case of plano-convex lens.

Figure 4 shows the corresponding distributions of optical retardation derived from fringe pattern with the highest optical retardation occurring near the gate. And Fig. 4 also shows an increase in retardation at the far end from gate in which the cross-section changes abruptly. As for birefringence distributions in gap-wise direction as shown in Fig. 5, it is noted that birefringence peaks not only at mold wall but also near the central part of lens thickness. The rationale is that the peak near the mold wall is due to the alignment of molecular chain frozen instantly near the surface during the filling stage. At the holding stage, more melt is packed into the lens gate through narrowing channel caused by the development of frozen layer; hence, the second peak appears near the central part of lens thickness.

DOE Analysis with Taguchi Methods

Adopted for studying causal effects between molding conditions and lens qualities, such as residual birefringence caused by shear stresses, the Taguchi Methods are employed for DOE procedures with the results given by CAE simulations and the profile measurements of molded lenses. The objective is to identify not only the effects of dominant processing parameters but also interactions among the parameters in a systematic approach [6,7]. Based upon the results reported by Wang and Lai [3,4], shear stresses are independent of the four interactions of holding pressure with injection speed, mold temperature, melt temperature, and cooling time, respectively. Rather, shear stresses are mainly influenced by melt temperature and injection speed alone. As for the results on average volumetric deviations, it mainly depends on holding pressure and melt temperature, respectively.

Due to the simple geometry of plano-convex spherical lens, the profile accuracy of the molded lenses was readily measured. When the lenses were molded, five main factors, namely melt temperature, mold temperature, injection speed, holding pressure, and cooling time were set at three levels based upon the Taguchi Methods. Moreover, four interactions of parameters on melt temperature with mold temperature, injection speed, holding pressure, and cooling time, respectively were also accounted in the experiments. All the samples were injected on a machine, Model 50i α made by Fanuc Co., Japan. Then, the profile accuracy of the molded lenses was measured by a profiler Form Talysurf, developed by Rank Taylor Hobson Limited, UK. For data comparisons, a statistical method is employed for analysis of data on the causal effects between the profile accuracy and processing parameters.

In the process of Taguchi analysis, specific types of S/N ratio are applied for corresponding specific purposes. In this study, P-V value should be selected as measure of profile accuracy and effectively minimized by proper process parameter settings. Hence, the S/N ratio for meeting the above requirement is smaller-the-better (STB) rule. Based upon the analysis results, it is noted that profile accuracy is mainly affected by mold temperature and melt temperature plus holding pressure interactions. Profile accuracy can be improved by increase of the melt temperature. The rationale is higher melt-temperature would make the polymer melt less likely to freeze quickly. Hence, the molded lenses get better packing effects and good profile accuracy. As for the effects of interactions, melt temperature plus holding pressure have greater influences than other interactions. Thus, the settings of both melt temperature and holding pressure should simultaneously be adjusted so that better profile accuracy can be obtained.

Experimental Verifications

For experimental verifications, Fig. 6 shows the photographic picture of the corresponding birefringence measurements at the monitored locations. Based upon the Stress-Optic Law, the gap wise average residual birefringence is described as follows

$$\Delta n = \frac{\lambda N}{h} = N, \quad (9)$$

Where Δn is the birefringence expressed into retardation; λ is the wavelength of light source (standard yellow at 589.3nm); N is the fringe order; h is the thickness of sampled location and a function of distance to lens gate. The calculated results given by Eq. (9) along the monitored path are plotted in Fig. 7.

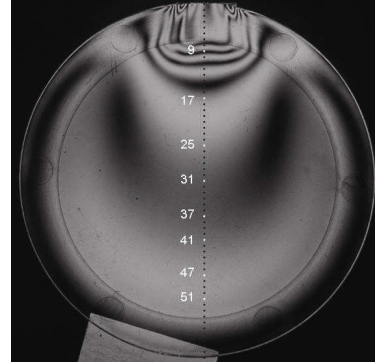


Fig. 6 Photographic picture showing the molded sample-lenses being measured for photo-elasticity values by linear-interpolation method.

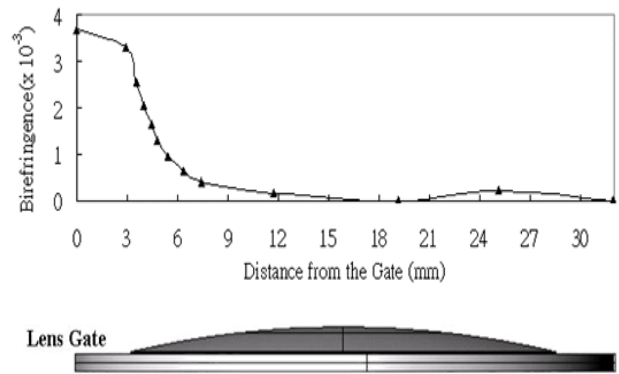


Fig. 7 Plots of distributions of residual birefringence measured along the filling path with the measurement error being smaller than 10%.

In Fig. 8, the photographically animated fringe patterns of plano-convex lens obtained from simulated predictions under a circular polariscope are compared with the photographic pictures taken from the corresponding experimental results. The figures clearly indicate that both simulated and experimental residual birefringence decreases along the flow path and reaches its highest values at the gate area and the sharp corners near the gate area. In addition, both simulated and experimental results from Fig. 4 and Fig. 8 show an increase in birefringence at the cross-sectional area with abrupt change in thickness circled in the figure. In terms of fringe order counts, the maximum fringe-count in sample lenses observed under the circular polariscope is 5 as compared to 4 from the simulated results. That is to say simulated results predicted less birefringence compared with the experimental observations.

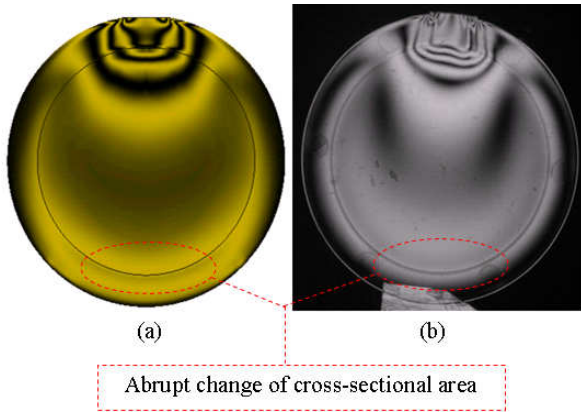


Fig. 8 Comparisons of fringe patterns on photographic pictures for the plano-convex sample lenses; (a) 3D CAE predictions based on the White-Metzner Model; (b) experimental photo-elasticity measurements.

In addition to good agreement between simulated and experimental fringe patterns, the predicted birefringence distributions at the gate area in the gap-wise direction also needs to be confirmed by experimental verifications. A conventional layer-removal technique was adopted for removing layers of molded samples. In the experiments, four samples of molded lenses with the same process conditions were carefully machined via diamond turning process in layer-thickness of 0.1 mm, 0.2 mm, 0.3 mm and 0.4 mm, respectively. Figure 9 compares the photographic pictures of residual birefringence under various removed layers of thickness. In Fig. 9(b), fringe-pattern of residual birefringence changes significantly after the first 0.1 mm layer was removed.

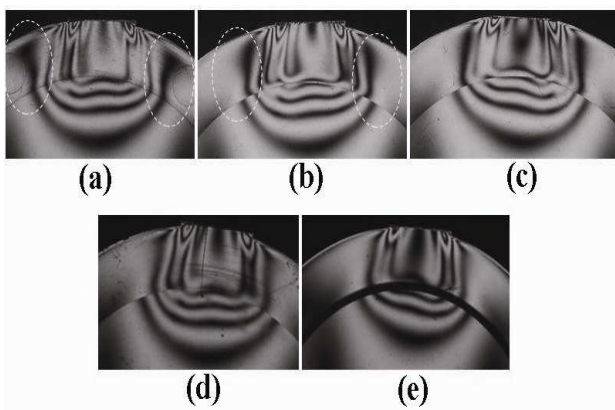


Fig. 9 Photographic pictures of fringe patterns due to residual birefringence on lens samples prepared by the layer-removal technique; (a) before machining, (b) 0.1 mm removed, (c) 0.2 mm removed, (d) 0.3 mm removed, (e) 0.4 mm removed.

For further illustrations on the changes of residual birefringence in gap-wise direction, the average fringe order of the samples was counted as shown in Table 2 and plotted in percentile of total removal as shown in Fig. 10. It is noted that nearly 30% of residual birefringence in gap-wise direction was removed on the first 0.1 mm layer of materials; and, the second peak of residual birefringence may occur between 0.2 mm and 0.3 mm of the removed layers. Whereas, the second peak of residual birefringence is accurately predicted by CAE simulations with the White-Metzner Model as shown in Fig. 5. Evidently, the second peak of birefringence is introduced by the packing flow of materials during the holding stage. As supported by the simulations, 50 % of the total birefringence was removed after 0.4 mm, namely half of gate thickness, layer of thickness was machined off.

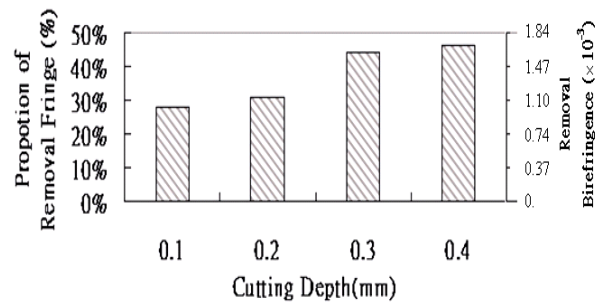


Fig. 10 Bar chart for percentile representation of removed birefringence versus layer thickness removed from the surface near the gate area.

Table 2 Average removal proportion of fringe order for different machining depths

Removal Depth (mm)	0	0.1	0.2	0.3	0.4
Average removal of fringe order (%)	0	27.9	30.8	43.9	46.2

Summary

In this paper, a truly three-dimensional CAE analysis based upon White-Metzner Model is investigated for representing the visco-elastic effects of polymeric flows in injection molding of optical parts. Residual birefringence in the molded lenses is predicted by converting the stresses into optical retardation given by Stress-Optic Law. Furthermore, birefringence distributions in both the gap-wise and flow direction are predicted by CAE simulations. For experimental verifications, photo-elasticity measurements are conducted for some cases with good agreement in the distribution values. In summary,

residual birefringence in injection-molded optical parts could be calculated with the proposed scheme; and, it is found to be mostly affected by melt temperature and injection speed during the complete cycle. Moreover, in injection molding of COC resins, the flow stresses during the filling and packing stage seem to be the dominant factor contributing to final residual birefringence although the thermal stresses may not be neglected during the cooling stage.

Birefringence of Injection Molded Parts,” *Proceedings of the Polymer Processing Society, 24th Annual Meeting*, Salerno, Italy (2008).

Key Words: Injection Molding, Plastics Lens, Birefringence, Taguchi Methods.

Acknowledgements

This research work is financially supported by the National Science Council in Taiwan, the Republic of China, under Contract No. NSC96-2221-E007-091.

References

1. Yoon, K., An Experimental Study on Precision Injection Molding of Center-Gated Disks, *Korean Journal of Rheology*, **7**, 19-27 (1995).
2. Shyu, G. D., Isayev, A. I., and Lee, H. S., Numerical Simulation of Flow-induced Birefringence in Injection Molded Disk, *Korea-Australia Rheology Journal*, **15**, 159-166 (2003).
3. Wang, P. J. and Lai, H. E., Study of Optical Characteristics for Injection Molded Aspheric Lenses, *Asia Pacific Conference on Optics Manufacture*, (2007).
4. Wang, P. J. and Lai, H. E., Study of Residual Birefringence in Injection Molded Lenses, *Plastics Encounter at ANTEC 2007*, 2494-2498 (2007).
5. CoreTech System, Moldex3D Overview, <http://www.moldex3d.com/en/index.php>.
6. Lu, X. H. and Khim, L. S., A Statistical Experimental Study of the Injection Molding of Optical Lenses, *Journal of Materials Processing Technology*, **113**, 189-195 (2001).
7. Montgomery, D. C., Design and analysis of experiments, Fifth Edition. John Wiley and Sons, Inc., New York, 60-132 (2001).
8. Wang, P. J. and Lai, H. E., Experimental Verifications of CAE Predictions on Birefringence of Injection Molded Lenses, *Plastics Encounter at ANTEC 2008*, 421-425 (2008).
9. Chang, Y. J., Yang, W. H., Hsu, C. H., and Chang, R. Y., “Integrated Numerical Simulations to Predict